Resistor-Network Formulation of Multi-Temperature Forced Convection Problems

Sepehr Foroushani[1] and John L. Wright[2]
University of Waterloo, Waterloo, ON, N2L 3G1, Canada

and

David Naylor[3]
Ryerson University, Toronto, ON, M5B 2K3, Canada

Foroushani, S., Naylor, D., & Wright, J. L. (2016). Resistor-Network Formulation of Multitemperature Forced-Convection Problems. Journal of Thermophysics and Heat Transfer, 1–8. https://doi.org/10.2514/1.T4993

[1] PhD Candidate, Department of Mechanical & Mechatronics Engineering
[2] Professor, Department of Mechanical & Mechatronics Engineering
[3] Professor, Department of Mechanical & Industrial Engineering

Resistor-Network Formulation of Multi-Temperature Forced Convection Problems

Sepehr Foroushani[4] and John L. Wright[5]
University of Waterloo, Waterloo, ON, N2L 3G1, Canada

and
David Naylor[6]
Ryerson University, Toronto, ON, M5B 2K3, Canada

Many convection heat transfer problems involve more than two isothermal heat sources/sinks. A network of multiple convective resistors connecting temperature nodes representing the isothermal sources (walls, inlet flows, *etc*.) can be used to represent this class of problem. However, the convective resistances that characterize this network cannot generally be evaluated using energy balances resulting from a solution to the energy equation. A technique based on solutions of the energy equation with perturbed boundary conditions is developed to overcome this difficulty. The resulting technique is verified by comparison with energy-balance results previously obtained for a special symmetric case. The technique is also applied to a superposition solution for hydrodynamically-developed laminar flow in an annulus and to numerical solutions of simultaneously-developing flow in an asymmetrically-heated annulus under both laminar and turbulent flow conditions. This work is part of an ongoing research project on the resistor-network modeling and characterization of multi-temperature convection problems.

Nomenclature

A = surface area [m^2]

C_n = series solution coefficient [-]

D_h = hydraulic diameter [m]

[4] PhD Candidate, Department of Mechanical & Mechatronics Engineering
[5] Professor, Department of Mechanical & Mechatronics Engineering
[6] Professor, Department of Mechanical & Industrial Engineering

f_n = eigenfunction [-]

H = channel width [m]

k = thermal conductivity [W/mK]

$\overline{Nu}$ = average Nusselt number [-]

Pr = Prandtl number [-]

q = heat flux [W/m^2]

Q = heat transfer rate [W]

r = radius/radial location [m]

$\bar{r}$ = dimensionless radius: $\bar{r}=r/r_1$ [-]

R = thermal resistance [K/W]

Re = Reynolds number based on hydraulic diameter [-]

S = conduction shape factor [m]

T = temperature [K]

$T^{(2T)}$ = two-temperature fundamental solution from ref [8] [K]

x = streamwise coordinate [m]

X = inverse Graetz number (Eq. 11) [-]

$\bar{y}$ = dimensionless lateral coordinate: $\bar{y}=y/H$ [-]

Greek Symbols

θ = dimensionless temperature [-]

λ_n = eigenvalue [-]

φ = radius ratio: $\varphi=r_2/r_1$ [-]

Subscripts

0 = (inlet) fluid

1 = upper/outer wall

2 = lower/inner wall

i = designates heated wall

ij = paired – from node i to node j

Superscripts

* = denotes perturbed condition

I. Introduction

Heat transfer problems are traditionally formulated in terms of a driving temperature difference and a corresponding heat transfer coefficient. In many cases, however, there are more than two temperatures involved and, hence, more than one temperature difference driving the heat transfer. Forced convection examples include heat transfer in asymmetrically-heated passages and in flow over nearby bodies with isothermal surfaces. In these cases, heat transfer between each pair of isothermal "sources" (surfaces and free-stream or inlet flows) is driven by the difference between the respective temperatures.

Nevertheless, characterizing the entire multi-temperature configuration in terms of a single heat transfer coefficient requires an "equivalent" or "effective" temperature difference. In flow in an asymmetrically-heated channel, for example, heat transfer is governed by three temperatures: the inlet flow temperature and the two wall temperatures. But to define a heat transfer coefficient, an effective temperature difference is constructed using the mean wall temperature and the bulk fluid temperature. In this case a temperature ratio is defined to specify the ordering of the inlet temperature with respective to the wall temperatures. The resulting heat transfer coefficient will depend on this temperature ratio. Shortcomings of this approach are discussed in detail in reference [1]. A major shortcoming is that it does not give the "split" of heat (transfer) between different sources. While the total heat transfer at the walls and the total heat transfer to the fluid can be calculated, it *cannot* be determined what portion of heat transfer at a wall goes to the fluid and what portion to the other wall. This will be demonstrated.

An alternative to the traditional approach is the use of a thermal-resistor network: multiple thermal resistors connecting temperature nodes that represent the isothermal sources. Each resistance corresponds to heat transfer between a specific pair of nodes. With the (multiple) paired resistances characterizing the network known, the split of heat transfer between the nodes can be readily calculated. This approach has been established for modeling convective heat transfer in building energy simulation. The resistor-network approach is computationally advantageous in time-step simulations since it provides the opportunity to model heat transfer a high level of detail and at a very low computational expense [2,3]. The utility of this approach has also been demonstrated [1] for the classical multi-temperature convection problem of fully-developed laminar flow in an asymmetrically-heated channel, the asymmetric Graetz problem. The resistor-network formulation has been shown to lead to a simpler representation of the solution, while revealing new details about the heat transfer phenomenon.

In the present paper, the formulation of three-temperature convection problems in terms of a resistor network is examined. It is shown that, except for special symmetric cases, the nodal energy balances obtained from solutions to the energy equation (or measurements) are not sufficient to yield the paired resistances that characterize the network. Nevertheless, an additional equation can be generated from the solution of the energy equation with perturbed boundary conditions. This additional equation is used to supplement the nodal energy balances and obtain the convective resistances. The proposed technique is verified by comparison with the energy-balance results previously obtained for the asymmetric Graetz problem. The technique is then applied to a variation of the asymmetric Graetz problem: forced convection in an asymmetrically-heated annulus – another benchmark problem. An existing analytical solution for hydrodynamically-developed, laminar flow is first considered. The analysis is then extended to CFD solutions of flows, both laminar and turbulent, with simultaneous hydrodynamic and thermal development.

This work is part of an ongoing research project on the modeling and characterization multi-temperature convection problems which are of special interest in building energy simulation.

II. Methodology – Part 1: The dQdT Technique

To illustrate the resistor-network formulation, consider a three-temperature convection problem, *e.g.* hydrodynamically-developed flow in an asymmetrically-heated annulus shown schematically in Figure 1. To represent this problem a delta network of three resistors (also shown in Figure 1) connecting the three temperature nodes representing the two annulus walls and the inlet flow can be used. Note that the fluid flow is represented by the inlet temperature – the corresponding independent boundary temperature.

The set of heat transfer rates, $\{Q_i\}$, can be calculated for any given set of boundary temperatures, $\{T_i\}$. But heat transfer at a node, say Q_2, is split between the two legs of the network connected to that node. See Equation 1 and the delta network of Figure 1.

$$Q_2 = Q_{20} + Q_{21} \tag{1}$$

Following the standard electrical analogy for heat transfer, the two paired heat transfer component on RHS of Equation 1 can be written in terms of the corresponding driving temperature difference and paired resistance. The term “paired” is used here to emphasize that R_{ij} corresponds to heat transfer between a specific pair of nodes, T_i and T_j. See Equation 2.

$$Q_{ij} = \frac{T_i - T_j}{R_{ij}} \tag{2}$$

Equation 1 can now be recast in terms of the three nodal temperatures, and the paired resistances connected to node 2. See Equation 3.

$$Q_2 = \frac{T_2 - T_0}{R_{20}} + \frac{T_2 - T_1}{R_{21}} \tag{3}$$

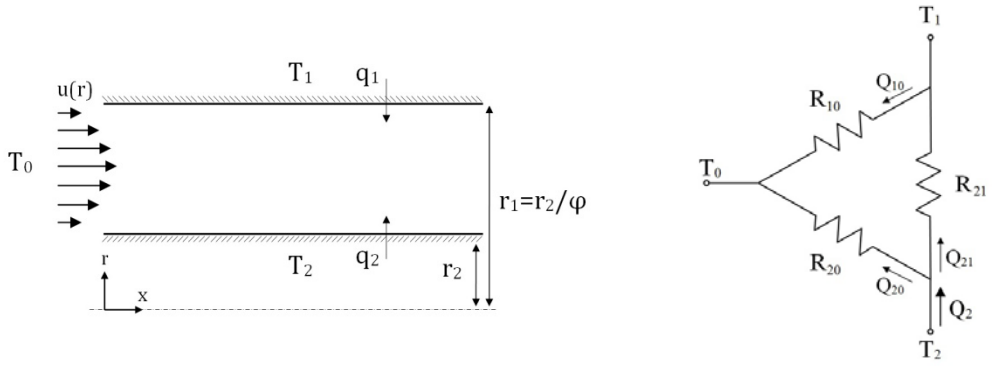

Figure 1: Schematic and resistor network of hydrodynamically-developed flow in an asymmetrically-heated annulus.

Writing an energy balance similar to Equation 3 for the other two nodes, three algebraic equations are obtained with the three resistances, $\{R_{ij}\}$, unknown. But these equations are not independent; they are interconnected by the overall energy balance of the network: $Q_0+Q_1+Q_2=0$. The system of equations is under-defined with three unknowns and only two independent equations. It is therefore not possible to determine the paired convective resistances (and thus the split of heat transfer at each node) based on the knowledge of the total heat transfer rates only. An additional equation is required.

If one of the temperatures, say T_1, is perturbed by δT_1, Q_2 will change as a result by some amount δQ_2. These changes are shown in Equations 4 and 5, where asterisks are introduced to designate the perturbed condition.

$$T_1^* = T_1 + \delta T_1 \tag{4}$$

$$Q_2^* = Q_2 + \delta Q_2 \tag{5}$$

The energy balance (Equation 3) can also be applied to the perturbed condition, as shown in Equation 6.

$$Q_2^* = \frac{T_2 - T_0}{R_{20}^*} + \frac{T_2 - T_1^*}{R_{21}^*} \tag{6}$$

It is important at this stage to recognize that a convective resistance is a function of only geometry, the velocity field and the fluid properties. Hence, for any given annulus, a change in T_1 could change both R_{20} and R_{21} through temperature-dependent fluid properties or thermal effects on the velocity field, *e.g.* buoyancy. Nevertheless, in a constant-property forced-convection problem, there is a one-way coupling between the velocity field and the temperature field. The convective resistances are thus independent of temperature, *i.e.* $R_{ij}^{*}=R_{ij}$. In other words, δQ_2 is caused by the change in the driving temperature difference solely. Equation 6 can be rewritten as shown in Equation 7.

$$Q_2^{*} = \frac{T_2 - T_0}{R_{20}} + \frac{T_2 - T_1^{*}}{R_{21}} \tag{7}$$

Equation 7 is the additional equation that closes the system; $\{R_{ij}\}$ can now be obtained. Subtracting Equation 3 from Equation 7, for example, R_{21} is found as shown in Equation 8.

$$R_{21} = -\frac{\delta T_1}{\delta Q_2} \tag{8}$$

In a constant-property forced-convection problem, the energy equation is linear with respect to temperature. Hence Equation 8 can be written in the differential form shown in Equation 9.

$$\frac{1}{R_{ij}} = -\frac{\partial Q_i}{\partial T_j} \tag{9}$$

As will be subsequently demonstrated, this differentiation can be done analytically for simple convection problems which have analytical solutions. For more complex flows, where an analytical solution is not at hand, the differentiation can be performed by perturbing the temperature boundary conditions in a numerical solution.

For convenience, the proposed technique which gives a paired resistance as the ratio between δQ and δT is dubbed dQdT. The main utility of the dQdT technique is that it provides a means of resolving the split of heat transfer in multi-temperature problems. With $\{R_{ij}\}$ obtained using dQdT, $\{Q_{ij}\}$ as well as $\{Q_i\}$ can be calculated for any $\{T_i\}$. This is new information which provides insight into the physics of the problem, and is not available in the traditional formulation.

III. Verification:

Hydrodynamically-Developed Laminar Flow in an Asymmetrically Heated Channel

Recall that R_{ij} is a function of geometry, the flow field and the fluid properties. In the special case of constant-property, hydrodynamically-developed, laminar flow in a flat-plate channel, the two wall-to-fluid resistances (R_{10} and R_{20}) are equal due to symmetry. The number of the unknowns is therefore reduced to two and the system of energy-balance equations can be solved for $\{R_{ij}\}$. In a recent paper [1], the analytical solution by Hatton and Turton [4] was used to derive expressions for $\{R_{ij}\}$. For the purpose of verification, the dQdT technique is applied here to obtain $\{R_{ij}\}$ of the same problem. A schematic of this configuration is shown in Figure 2. Note that this configuration is a limiting case of flow in an asymmetrically-heated annulus with a radius ratio approaching one. The results obtained in [1] by equating the two wall-to-fluid resistances, $R_{10}=R_{20}$, and solving the nodal energy balances are used here to validate the dQdT results.

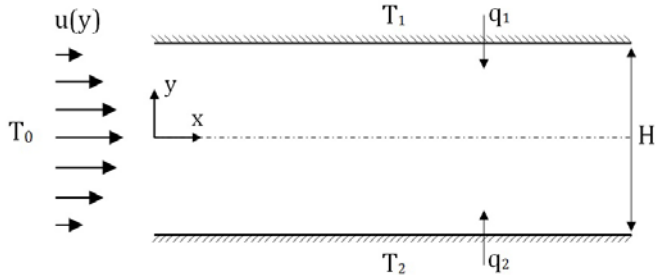

Figure 2: Schematic of hydrodynamically-developed flow in an asymmetrically-heated channel [1].

To apply dQdT, *i.e.* perform the partial differentiation of Equation 9 to get $\{R_{ij}\}$, the solution by Hatton and Turton [4] was used to obtain expressions for $\{Q_i\}$. Hatton and Turton presented a series solution to the energy equation in terms of the dimensionless temperature $\theta = (T - T_{wm})/(T_1 - T_{wm})$, in the form of Equation 10.

$$\theta = \left(\frac{2y}{H}\right) - \sum_{n=1}^{\infty} C_n f_n \exp\left(-\frac{8}{3}\lambda_n^2 X\right) \tag{10}$$

In Equation 10, the first term on RHS is the linear, fully-developed temperature profile, and the summation is the series solution to a Sturm-Liouville system, with C_n, f_n and λ_n denoting the coefficients, the eigenfunctions and the eigenvalues, respectively. X is the inverse Graetz number, defined in Equation 11, representing streamwise coordinate along the channel.

$$X = \frac{x}{H/2} \cdot \frac{1}{Re \cdot Pr} \tag{11}$$

With the temperature distribution known heat flux at each wall was obtained by differentiation, resulting in Equation 12.

$$q_i = -\frac{k}{H}(T_1 - T_2)\left(\frac{\partial\theta}{\partial\bar{y}}\right)_{\bar{y}_i}$$

$$= -\frac{k}{H}(T_1 - T_2)\left[1 - \sum_{n=1}^{\infty} C_n \left(\frac{df_n}{d\bar{y}}\right)_{\bar{y}_i} \exp\left(-\frac{8}{3}\lambda_n^2 X\right)\right] \qquad i=1,2 \qquad (12)$$

Equation 12 was then integrated from the channel entrance to location x, to find the (per-unit-depth) total heat transfer rates, Q_1 and Q_2. See Equation 13.

$$Q_i = \int_0^x q_i\, dx = -\frac{k}{H}(T_1 - T_2) \int_0^x \left[1 - \sum_{n=1}^{\infty} C_n \left(\frac{df_n}{d\bar{y}}\right)_{\bar{y}_i} \exp\left(-\frac{8}{3}\lambda_n^2 X\right)\right] dx \qquad (13)$$

To have the results in terms of X only, the integral can be evaluated using a change of variable as shown in Equation 14.

$$\int \left[\sum_{n=1}^{\infty} C_n \left(\frac{df_n}{d\bar{y}}\right)_{\bar{y}_i} \exp\left(-\frac{8}{3}\lambda_n^2 X\right)\right] dx$$

$$= \mathrm{Re}\cdot\mathrm{Pr}\left(\frac{H}{2}\right) \sum_{n=1}^{\infty} \left\{C_n \left(\frac{df_n}{d\bar{y}}\right) \int \exp\left(-\frac{8}{3}\lambda_n^2 X\right) dX\right\}$$

$$= \mathrm{Re}\cdot\mathrm{Pr}\left(\frac{H}{2}\right) \sum_{n=1}^{\infty} \left\{-\frac{3C_n}{8\lambda_n^2}\left(\frac{df_n}{d\bar{y}}\right) \exp\left(-\frac{8}{3}\lambda_n^2 X\right)\right\} \qquad (14)$$

The resulting expressions for $\{Q_i\}$ were then differentiated with respect to $\{T_i\}$ to obtain $\{R_{ij}\}$ according to Equation 9. Average paired Nusselt numbers, defined as shown in Equation 15, are used here to report the results in dimensionless form.

$$\overline{Nu_{ij}} = \left[\frac{Q_{ij}}{(T_i - T_j)x}\right]\frac{H}{k} = \left(\frac{1}{R_{ij}x}\right)\frac{H}{k} \qquad (15)$$

Equations 16 and 17 are the dQdT results based on the eigenvalues and eigenfunction derivatives reported by Hatton and Turton.

$$\overline{Nu_{12}} = \frac{1}{X}(X - 0.2 + 0.2276e^{-7.54X} - 0.0367e^{-35.96X} - 0.0133e^{-85.73X} - 0.0066e^{-156.83X} + 0.0038e^{-249.27X} - 0.0025e^{-363.04X} + 0.0017e^{-498.15X} - 0.0012e^{-654.59X} + 0.0009e^{-832.39X} - 0.0001e^{-1031.47X} + 0.0006e^{-1251.93X} - 0.0005e^{-1493.69X} + 0.0004e^{-1756.80X} - 0.0003e^{-2041.25X} + 0.0003e^{-2347.03X} - 0.0002e^{-2674.81X}) \quad (16)$$

$$\overline{Nu_{10}} = \overline{Nu_{20}} = \frac{1}{X}(0.5 - 0.4552e^{-7.54X} - 0.0266e^{-85.73X} - 0.0076e^{-249.27X} - 0.0034e^{-498.15X} - 0.0019e^{-832.39X} - 0.0012e^{-1251.93X} - 0.0008e^{-1756.80X} - 0.0006e^{-2347.03X}) \quad (17)$$

Comparing Equations 16 and 17, obtained by dQdT, with the expressions reported in [1], found by solving equating R_{10} and R_{20} and solving the nodal energy balances, it can be seen that they are identical. The dQdT technique for calculating the paired resistances is thus verified.

The two sets of results are plotted in Figure 3. Wall-to-fluid heat transfer is singularly high at the inlet and decays to zero well downstream of the channel inlet as the two boundary layers merge and the flow reaches thermal development. Wall-to-wall heat transfer is zero at the inlet and grows to the pure-conduction limit at $X \rightarrow \infty$. See reference [1] for a detailed discussion of these results.

As discussed in reference [1], in addition to the split of heat transfer remaining unknown, the traditional formulation based on the bulk fluid temperature has other shortcomings when applied to asymmetrically-heated channels. Most notably: *i*) a non-physical singularity occurs in the distribution of one of the *local* Nusselt numbers at the point where the bulk fluid temperature reaches the temperature of the corresponding wall, and *ii*) the Nusselt numbers depend on temperature ratio, which is inconsistent with the physics of the problem. These problems are apparent in the results presented by Hatton and Turton [4] and Mitrovic *et al*. [5].The same problems are seen in results presented for asymmetrically-heated annuli using the traditional formulation, *e.g.* [6,7]. The resistor-network formulation and the corresponding paired convective resistances have been shown to address these shortcomings [1].

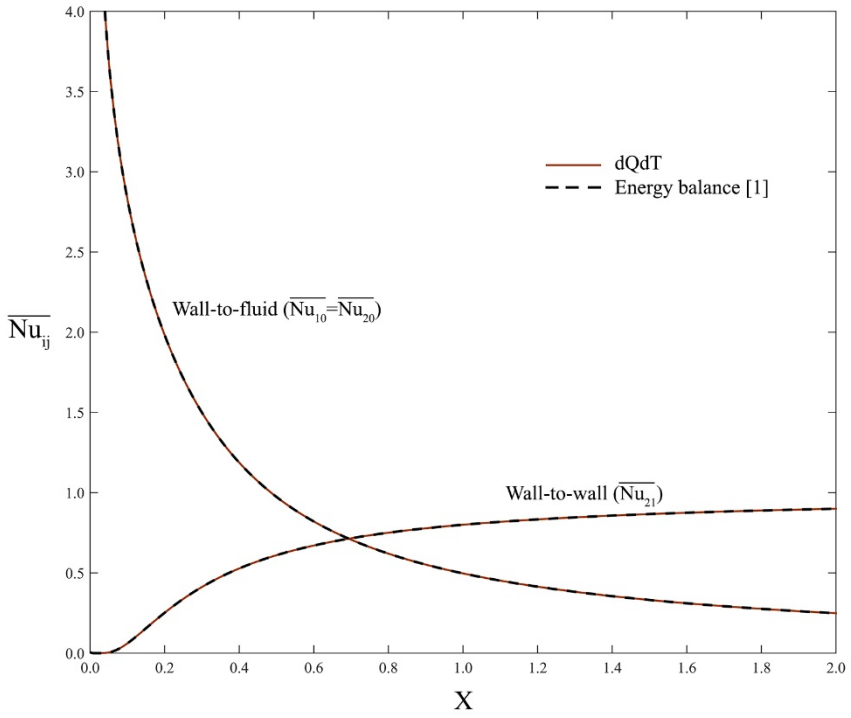

Figure 3: Average paired Nusselt numbers of hydrodynamically-developed laminar flow in a flat-plate channel obtained from nodal energy balances [1] and by dQdT.

IV. Sample Results – Part 1: Hydrodynamically-Developed Laminar Flow in an Asymmetrically-Heated Annulus

In this section, the dQdT technique is applied to an analytical solution for hydrodynamically-developed laminar flow in an annulus. In this case, due to asymmetry, the two wall-to-fluid resistances are not equal and the paired resistances cannot be found based only on the nodal energy balances. Sample dQdT results are presented and known limiting cases are examined to further validate the developed technique.

Lundberg *et al.* [8] solved the problem of constant-property, hydrodynamically-developed, laminar flow in asymmetrically-heated concentric annuli for the special case where one of the walls is maintained at the same temperature as the inlet flow and the other wall is heated to a second temperature. Similar to the solution by Hatton and Turton for channel flow, the solution by Lundberg *et al.* is expressed as the superposition of a one-dimensional solution for non-homogeneous boundary conditions (the fully-developed solution, θ_{fd}) and a series solution for homogeneous boundary conditions. See Equation 18.

$$\theta_i = \theta_{fd,i} - \sum_{n=0}^{\infty} (C_n)_i f_n \exp(-\lambda_n^2 X) \tag{18}$$

In Equation 18, $\theta_i = (T - T_0)/(T_i - T_0)$ is dimensionless temperature, and X is the inverse Graetz number defined similar to Equation 11 but with H/2 replaced with the annulus hydraulic diameter, $D_h=2(r_o-r_i)$. C_n, f_n and λ_n are, respectively, the coefficients, eigenfunctions and eigenvalues of the series solution for the "fundamental solution of the first kind," *i.e.* for Dirichlet conditions at the boundaries [8]. The subscript i denotes the heated wall: θ_2, for example, is the fundamental solution of the first kind for the case where the outer wall is at the same temperature as the inlet flow ($T_1=T_0$), while the inner wall is maintained at a different temperature (T_2). The fully-developed temperature profile, θ_{fd}, is given by Equation 19.

$$\theta_{fd,i} = \frac{\ln(r/r_j)}{\ln(r_i/r_j)} \tag{19}$$

Given the linearity of the energy equation and the boundary conditions, a solution to the generic case where the walls are at two different temperatures distinct from the inlet flow temperature – the "true" three-temperature problem – can be constructed using superposition. See Equation 20, where the solution to the three-temperature case, T, is expressed as the sum of the solution to a two-temperature case where the outer wall is heated, $T_1^{(2T)}$, and the solution to a two-temperature case where the inner wall is heated, $T_2^{(2T)}$. This is illustrated schematically in Figure 4.

$$T = T_1^{(2T)} + T_2^{(2T)} \tag{20}$$

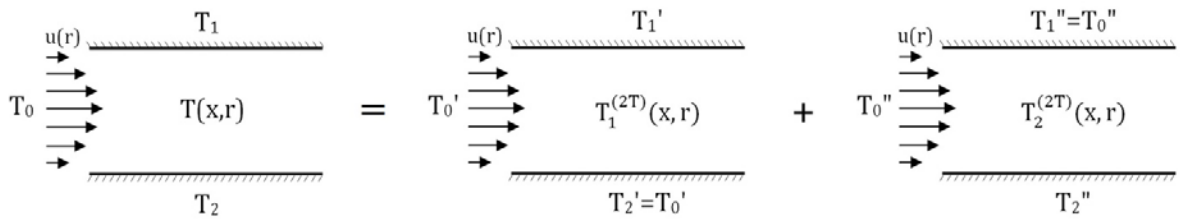

Figure 4: Generic three-temperature solution as superposition of fundamental two-temperature solutions.

With $T_i^{(2T)}$ known in dimensionless form (θ_i) from the work of Lundberg *et al.* and noting that superposition requires $T_i'+T_i''=T_i$, the three-temperature solution is obtained as shown in Equation 21.

$$T = (T_1 - T_0)\cdot\theta_1 + (T_2 - T_0)\cdot\theta_2 + T_0 \tag{21}$$

Differentiating Equation 21, wall heat fluxes are found as shown in Equation 22, where $\bar{r} = r/r_1$ is dimensionless radial location.

$$q_i = -k\left(\frac{\partial T}{\partial r}\right)_{r_i}$$

$$= -\frac{k}{r_1}\left[(T_1 - T_0)\left(\frac{\partial \theta_1}{\partial \bar{r}}\right)_{\bar{r}_1} + (T_2 - T_0)\left(\frac{\partial \theta_2}{\partial \bar{r}}\right)_{\bar{r}_2}\right] \tag{22}$$

Differentiating Equation 18, the gradient terms in Equation 22 can be written as shown in Equation 23.

$$\frac{\partial \theta_i}{\partial \bar{r}} = \frac{d\theta_{fd,i}}{d\bar{r}} - \sum_{n=0}^{\infty}\left\{(C_n)_i \frac{df_n}{d\bar{r}} \exp(-\lambda_n^2 X)\right\} \tag{23}$$

To evaluate the paired convective resistances, the wall heat fluxes are integrated to obtain total heat transfer rates, $\{Q_i\}$. The partial differentiation shown in Equation 9 is then performed to obtain the paired convective resistances. Results are reported in terms of average paired Nusselt numbers, defined in Equation 24. In this definition, a characteristic length of (r_1-r_2) is used to match the flat-plate channel results (based on H) in the $r_2/r_1 \to 1$ limit.

$$\overline{Nu}_{ij} = \left(\frac{1}{R_{ij}A_i}\right)\left(\frac{r_1 - r_2}{k}\right) \tag{24}$$

The resulting expressions are shown in Equations 25, 26 and 27 where $\varphi = r_2/r_1$.*

$$\overline{Nu}_{21} = \frac{(1-\varphi)}{X}\left[\frac{X/\varphi}{\ln(1/\varphi)} - \sum_{n=0}^{\infty}\left\{\frac{(C_n)_1}{-\lambda_n^2}\left(\frac{df_n}{d\bar{r}}\right)_{\bar{r}_2}\exp(-\lambda_n^2 X)\right\}\right] \tag{25}$$

$$\overline{Nu}_{10} = \frac{(1-\varphi)}{X}\sum_{n=0}^{\infty}\left\{\left[\frac{(C_n)_1 + (C_n)_2}{-\lambda_n^2}\right]\left(\frac{df_n}{d\bar{r}}\right)_{\bar{r}_1}\exp(-\lambda_n^2 X)\right\} \tag{26}$$

$$\overline{Nu}_{20} = \frac{(1-\varphi)}{X}\sum_{n=0}^{\infty}\left\{\left[\frac{(C_n)_1 + (C_n)_2}{-\lambda_n^2}\right]\left(\frac{df_n}{d\bar{r}}\right)_{\bar{r}_2}\exp(-\lambda_n^2 X)\right\} \tag{27}$$

Equations 25, 26 and 27 show that $\{Nu_{ij}\}$ does not depend on $\{T_i\}$ or some temperature ratio, which is consistent with the physics of a constant-property forced-convection problem. As discussed in reference [1], however, the traditional formulation based on the bulk fluid temperature leads to Nusselt numbers that depend on a temperature ratio characterizing the ordering of the wall temperatures and the inlet flow temperature.

---

* Note that in reference [8] non-zero values are given for $(1-\varphi)(C_n)_i$ with $\varphi \to 1$. Therefore, $\varphi = 1$ does not yield $\overline{Nu}_{ij}(X) = 0$.

Evaluating C_n, f_n and λ_n for any given φ and substituting the results in Equations 25-27, three universal curves are obtained that can be applied to any set of boundary temperatures ($\{T_i\}$), any laminar flow rate (Re) and any fluid (Pr). Sample results are plotted in Figure 5 for a radius ratio of φ=0.5. The coefficients, eigenvalues and eigenfunction derivatives given by Lundberg *et al.* [8] were used to evaluate $\{\overline{Nu_{ij}}\}$. Wall-to-fluid heat transfer is infinitely large at the annulus inlet, similar to the leading-edge singularity in flow over a flat plate: $\lim_{X\to 0} \overline{Nu_{i0}} \to \infty$. As the flow develops thermally, with the temperature profile approaching the fully-developed profile of Equation 19, wall-to-fluid heat transfer decreases, approaching a limiting value of zero at $X\to\infty$. The asymmetry in the geometry, *i.e.* the different curvature of the inner and outer walls, leads to a difference between the two wall-to-fluid Nusselt numbers. The surface with the lower curvature has a lower wall-to-fluid Nusselt number: $\overline{Nu_{12}} < \overline{Nu_{21}}$.

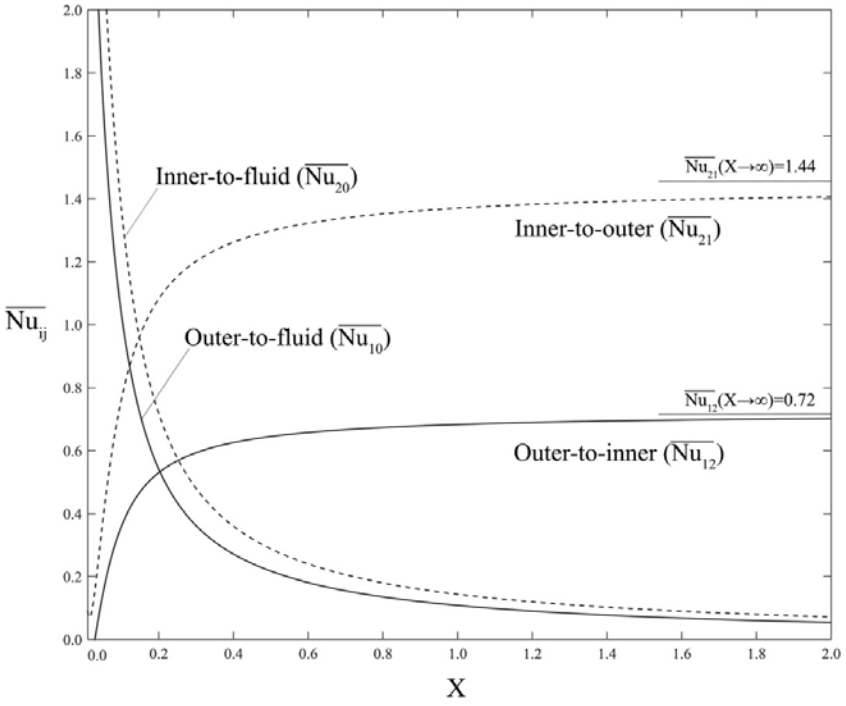

Figure 5: Average paired Nusselt numbers calculated using dQdT (fully-developed laminar flow, φ=0.5).

Wall-to-wall heat transfer, on the other hand, increases from zero at the inlet and to the pure-conduction limit. Note that $\overline{Nu_{12}}$ and $\overline{Nu_{21}}$ are not equal due to the difference between the respective areas; $\overline{Nu_{12}} / \overline{Nu_{21}} = \varphi = 0.5$. This result is expected since calculating the wall-to-wall heat transfer rate using either wall-to-wall Nusselt number,

the same result should be obtained: Q_{21}=-Q_{12}. The slight departure of $\overline{Nu_{12}}$ and $\overline{Nu_{21}}$ from zero at X=0 is because only the first four eigenvalues were used.

To demonstrate the validity of these results, two limiting cases may be considered. First: in the thermally-developed limit ($X\rightarrow\infty$), there is zero heat transfer between the annulus walls and the flow, hence: $\lim_{X\rightarrow\infty} \overline{Nu_{10}} = \lim_{X\rightarrow\infty} \overline{Nu_{20}} = 0$. Wall-to-wall heat transfer, on the other hand, approaches the pure-conduction limit with $\lim_{X\rightarrow\infty} \overline{Nu_{12}} = 0.72$. Using this limiting value, obtained by dQdT, the wall-to-wall heat transfer rate in a portion of length L in the thermally-developed region of the flow can be calculated as shown in Equation 28.

$$(Q_{12})_{fd} = \left(\lim_{X\rightarrow\infty} \overline{Nu_{12}}\right)\left(\frac{k}{r_1 - r_2}\right) A_1\ (T_1 - T_2)$$

$$= 9.064\ \ kL(T_1 - T_2) \tag{28}$$

The same result is obtained using $\lim_{X\rightarrow\infty} \overline{Nu_{21}} = 1.44$.

Alternatively, the wall-to-wall heat transfer rate in the pure-conduction limit can be calculated using the conduction shape factor of the annulus, $S=2\pi L/\ln(1/\varphi)$ which yields $S=9.065L$ for $\varphi=0.5$. The fully-developed wall-to-wall heat transfer rate is then obtained as shown in Equation 29. Comparing Equations 28 and 29 demonstrates the accuracy of the dQdT results.

$$(Q_{12})_{fd} = Sk(T_1 - T_2) = 9.065\ \ kL(T_1 - T_2) \tag{29}$$

The second case is the limit where the curvature of both annulus walls approaches zero; $\varphi\rightarrow 1$. In this limit, the solution to the annulus problem must approach the solution to the flat-plate channel problem. In Figure 6, the distribution of the dQdT results for the inner-to-fluid paired Nusselt number, $\overline{Nu_{20}}$, is plotted for various radius ratios. It can be seen that as $\varphi\rightarrow 1$, $\overline{Nu_{20}}$ approaches the wall-to-fluid Nusselt number of the channel problem, examined earlier. The slight discrepancy between the $\varphi\rightarrow 1$ curve and the channel-flow curve (dashed) is due to the difference between the two sets of eigenvalues (from references [4] and [8]) used to generate the respective curves.

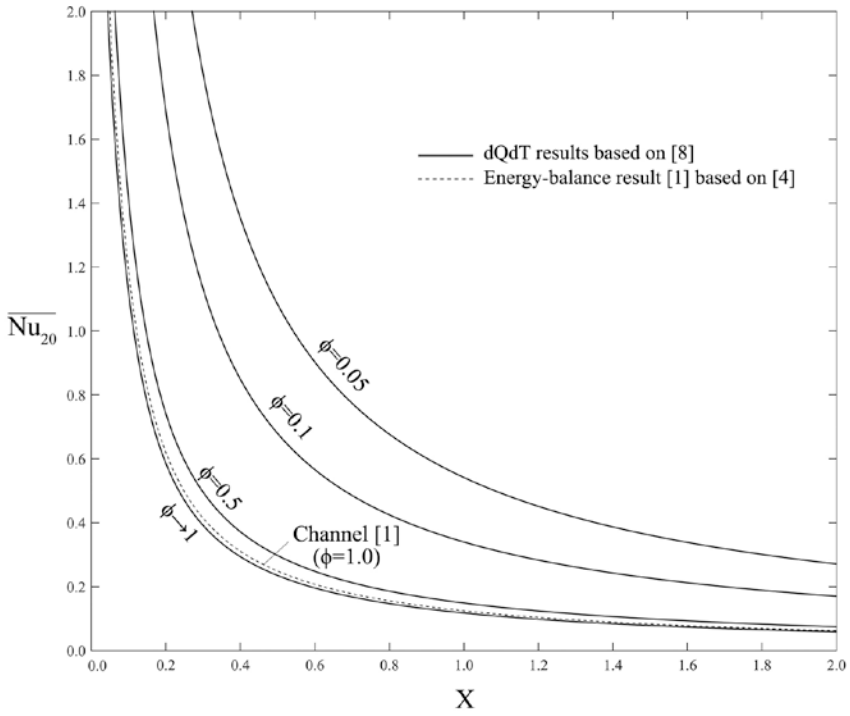

Figure 6: Average inner-wall-to-fluid Nusselt number for different radius ratios – $\varphi=r_2/r_1$ (fully-developed laminar flow).

V. Methodology – Part 2: Numerical Implementation of dQdT

In the previous section, an analytical solution for hydrodynamically-developed laminar flow in annuli was used to apply dQdT analytically. But analytical solutions are rarely available. No such solution for simultaneously-developing flow in an annulus was found. Numerical solutions, however, can be obtained relatively easily for different configurations and flow conditions. The dQdT technique for obtaining the paired convective resistances also can be applied numerically: the partial differentiation of Equation 9 can be evaluated using a numerical solution of the governing equations and subsequent solutions of the energy equation with perturbed boundary conditions.

Numerical implementation of dQdT is demonstrated and verified here using a numerical solution to the energy equation for hydrodynamically-developed, laminar flow in two geometries: the flat-plate channel and an annulus with $\varphi=0.5$. The commercial code ANSYS FLUENT 14.0 [9,10] was used to obtain 2nd-order, constant-property solutions to the complete, elliptic energy equation. This "baseline" solution was used to obtain the total heat transfer rates, $\{Q_i(x)\}$. Next, a boundary temperature T_j was changed to $T_j+\delta T_j$ and the energy equation was solved again to obtain the new transfer rates, $\{Q_i^*(x)\}$. $\{R_{ij}\}$ was then found using Equation 8. Note that due to the linearity of the

energy equation, the size of the perturbation is of no consequence. δT_j need only be large enough that the resulting $\{\delta Q_i\}$ can be detected within the numerical accuracy of the solution.

Results are plotted in Figures 7 and 8 in terms of the average paired Nusselt number defined in Equation 30.

$$\overline{Nu_{ij}} = \frac{1}{A_i}\left(\frac{Q_i - Q_i^*}{\delta T_j}\right)\frac{D_h/2}{k} \tag{30}$$

Analytical dQdT results presented in the previous sections are reproduced in Figures 7 and 8 for comparison. The results are in very close agreement with the largest discrepancy between the numerical and analytical dQdT results occurring in the vicinity of the inlet ($X \lesssim 0.1$). This near-inlet discrepancy is more pronounced for the annulus results (Figure 8). Note that the numerical results are obtained using a numerical solution to the full energy equation, while analytical results are based on a series solution to the simplified energy equation with axial diffusion neglected. Further note that the analytical results are based on only the first few terms of the series solutions.

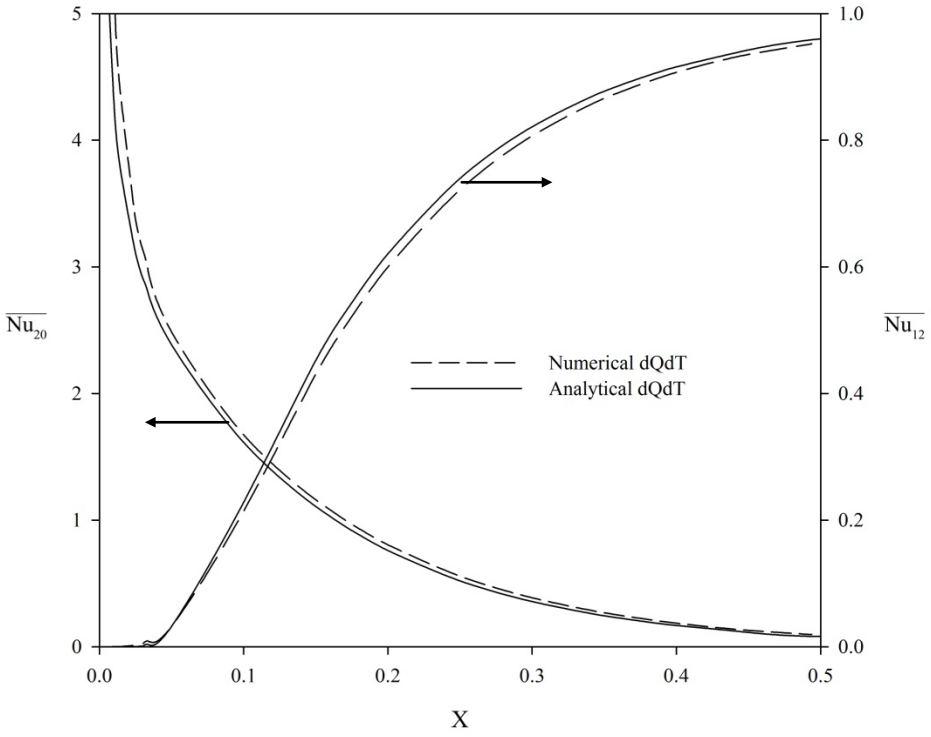

Figure 7: Average paired Nusselt numbers obtained using analytical and numerical dQdT (fully-developed laminar flow in channel).

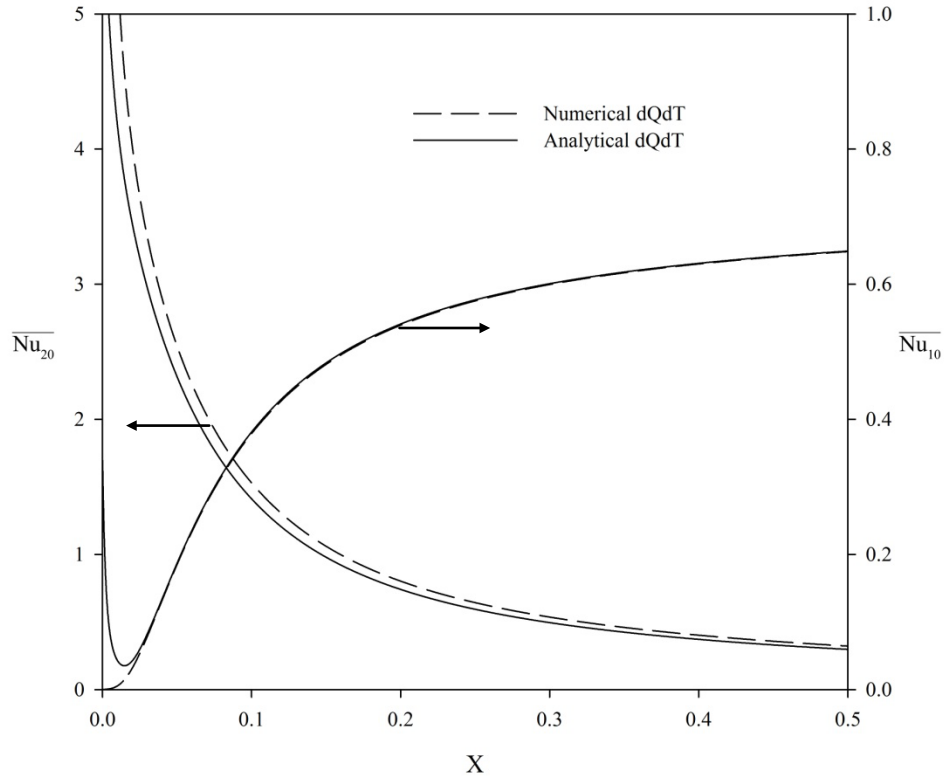

Figure 8: Average paired Nusselt numbers obtained using analytical and numerical dQdT (fully-developed laminar flow in annulus, φ=0.5).

VI. Sample Results – Part 2: Simultaneously-Developing Laminar or Turbulent Flow in an Asymmetrically-Heated Annulus

To demonstrate the general applicability of the dQdT technique, numerical dQdT was used to obtain the paired convective resistances of flows developing hydrodynamically and thermally in an asymmetrically-heated annulus with φ=0.5. Both laminar and turbulent flow cases were considered. ANSYS FLUENT 14.0 was used to obtain 2nd-order, constant-property solutions to the momentum and energy equations in an axisymmetric model of the annulus. The SIMPLE scheme was used to handle the pressure-velocity coupling. The shear-stress transport (SST) *k*-*ω* turbulence model was used for the fully turbulent cases.

A Richardson-extrapolation-based technique [11] was used to assess grid dependence of the solutions. Using three non-uniform rectangular grids with 28000, 53000 and 200000 control volumes, and based on the rate of total heat transfer to the fluid, Q_0, grid convergence indices of 1% and 2% respectively were found for the Re=50 and Re=10^4 cases. The apparent order of the solutions was found to be 2.

The baseline CFD solutions were validated against the experimental results of Roberts and Barrow [12] for simultaneously-developing flow of air (Pr=0.7) at Re=55000 in an annulus with φ=0.476, while the inner wall was heated with a uniform heat flux and the outer wall was insulated. As shown in Figure 9, the present numerical solution is in better agreement with the measurements of Roberts and Barrow than the results of an earlier numerical study by Malik [13]. Away from the inlet ($x>5D_h$) the present numerical results are less than 10% higher than the experimental data. Unfortunately, the turbulence intensity at the inlet and the uncertainty in the measurements of the wall Nusselt number are not reported by Roberts and Barrow [12]. It is stated that the flow is ensured to be fully turbulent by the use of tripping devices at the annulus entrance [12], but the inlet turbulence was not quantified, merely reported to be "small." In reference [13] an inlet turbulence intensity of 0.02% has been used. In the present CFD solutions inlet turbulence intensities between 0.02% and 1% were tested leading to less than 1% change in the average Nusselt number from x=0 to $x=15D_h$. Results shown in Figure 9 are for an inlet intensity of 1%.

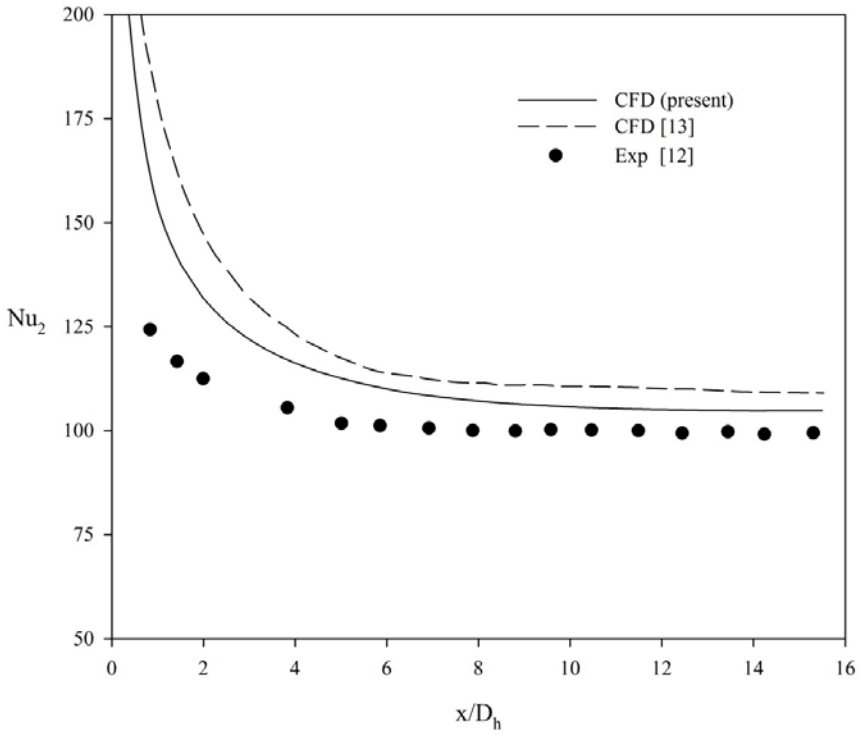

Figure 9: Inner-wall local Nusselt number for turbulent, developing flow in an annulus. Inner wall heated with uniform flux, outer wall insulated. (φ=0.476, Re=55000, Pr=0.7).

CFD-based dQdT can be used to evaluate the paired convective resistances for any fluid, any flow rate and any geometry (annulus radius ratio and eccentricity). Sample results of numerical dQdT are shown in Figures 10, 11 and

12 for the flow of air (Pr=0.7) in a concentric annulus with φ=0.5 at various flow rates, $10 \le Re \le 10^4$. A relatively high inlet turbulent intensity of 15% was used for the fully turbulent cases. Again, no dependence on temperature or temperature ratio is observed in the results.

Average outer-to-inner Nusselt number, plotted in Figure 10, starts from $\overline{Nu_{12}}=0$ at X=0 and approaches the pure-conduction limit of 0.72. As the flow rate increases, the thermal development of the flow is delayed and, therefore, $\overline{Nu_{12}}$ at any given location is decreased. In the fully turbulent cases (dashed curves), wall-to-wall heat transfer is enhanced by turbulent mixing. Therefore: $\overline{Nu_{12}}$ (Re=10^4) > $\overline{Nu_{12}}$ (Re=5000) > $\overline{Nu_{12}}$ (Re=1000). For simultaneously-developing flow too, $\overline{Nu_{21}} / \overline{Nu_{12}} = \varphi = 0.5$ in keeping with the idea that $Q_{12}=-Q_{21}$.

Wall-to-fluid Nusselt numbers, $\overline{Nu_{10}}$ and $\overline{Nu_{20}}$, are plotted in Figures 11 and 12. The general trend is similar to the hydrodynamically-developed case, starting from singularly high wall-to-fluid heat transfer at the annulus inlet and decaying as the flow develops thermally. Transition to turbulence significantly enhances wall-to-fluid heat transfer. Similar to the hydrodynamically-developed case, $\overline{Nu_{10}} > \overline{Nu_{20}}$.

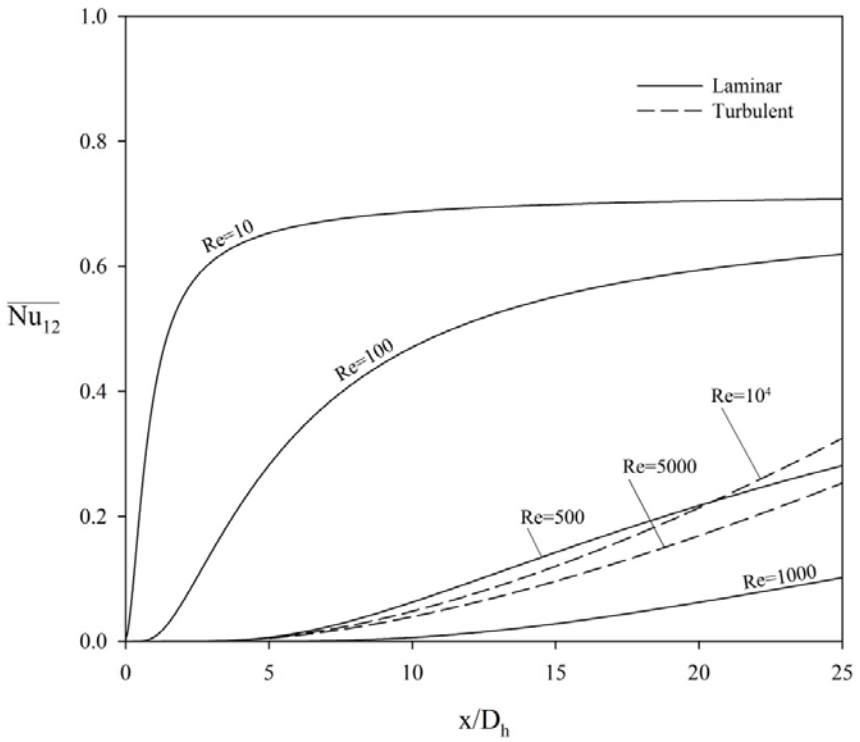

Figure 10: Average outer-wall-to-inner-wall Nusselt number in developing flow (φ=0.5, Pr=0.7)

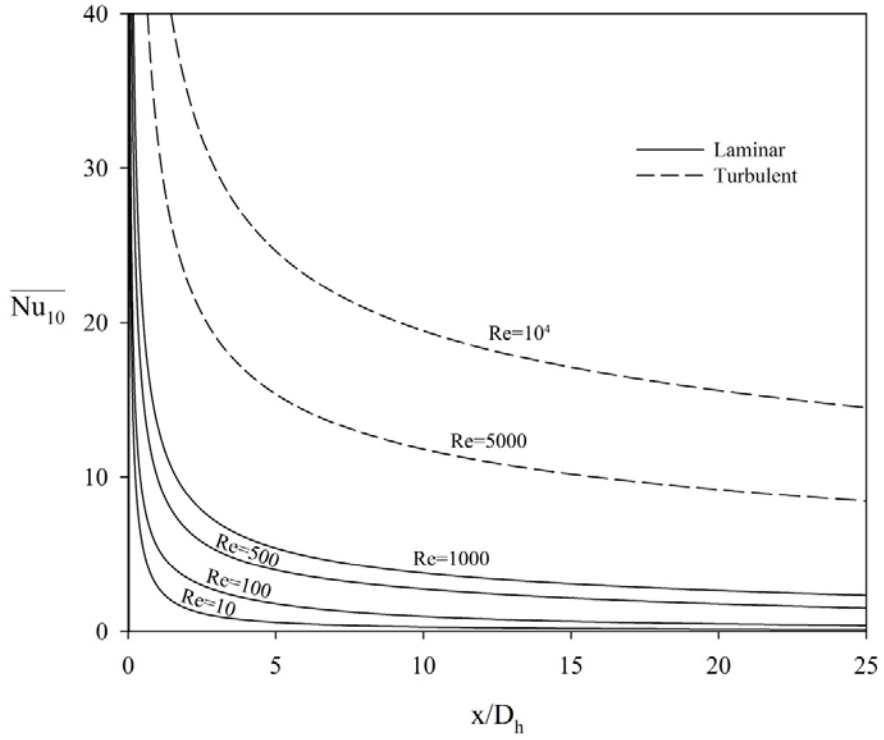

Figure 11: Average outer-wall-to-fluid Nusselt number in developing flow (φ=0.5, Pr=0.7).

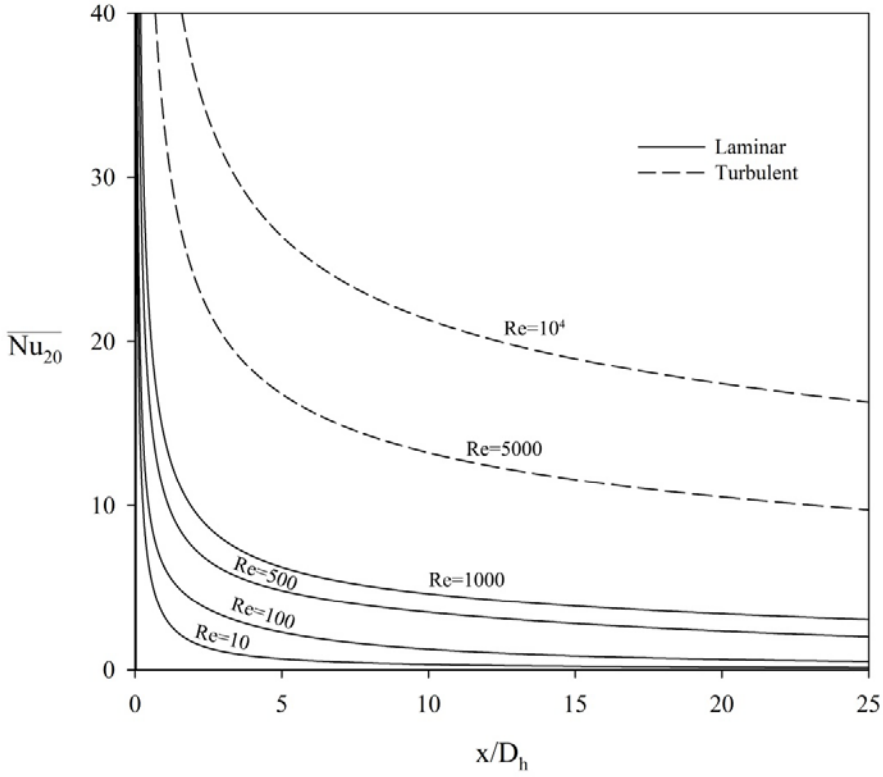

Figure 12: Average inner-wall-to-fluid Nusselt number in developing flow (φ=0.5, Pr=0.7).

VII. Conclusion

In many convection problems heat transfer occurs between more than two isothermal sources/sinks. In this paper the formulation of this class, (constant-property) multi-temperature forced convection problems, in terms of a network of thermal resistors was discussed. The most notable advantage of this approach is that it reveals the split of heat transfer between the sources – information not available in the traditional formulation. However, the evaluation of the paired convective resistances that characterize the resistor network of a multi-temperature problem is in general not possible based only on energy balances at the network nodes. A new technique (dQdT) entailing solutions of the energy equation with perturbed boundary conditions was developed to overcome this difficulty. The validity of the dQdT technique was established based on comparison to previous analytical solutions for special symmetric cases, and physical arguments.

The resistor-network approach and the dQdT technique were demonstrated for two benchmark three-temperature forced convection problems with existing analytical solutions: heat transfer in hydrodynamically-developed laminar flow in asymmetrically-heated channels and in asymmetrically-heated annuli. Next, numerical dQdT based on numerical solutions of the energy equation with perturbed boundary conditions was applied to the problem of simultaneously-developing flow in an asymmetrically-heated annulus, under both laminar and turbulent regimes. Physical explanations were given for the sample dQdT results presented and the trends observed. Some known limits were examined to support the results.

This work is part of an ongoing research project on the modeling and characterization of multi-temperature convection problems in terms of resistor networks. The resistor-network approach is of particular interest and utility in the field of building energy simulation. In this paper, only constant-property forced-convection problems were considered. However, given the demonstrated advantages of the resistor-network formulation, it is tempting to apply this approach to other multi-temperature convection problems. Extension of this work to the general problem of multi-temperature convection, including variable properties and free convection, will be presented in future work.

Acknowledgments

This work was funded by the Smart Net-Zero Energy Buildings Strategic Research Network (SNEBRN) of the Natural Sciences and Engineering Research Council of Canada (NSERC) and the University of Waterloo.

References

[1] Foroushani, S.S.M., Naylor, D., and Wright, J.L., "The asymmetric Graetz problem: The analytical solution revisited," *Thermophsyics & Heat Transfer*, 2016 [In press].

[2] Wright, J.L., Barnaby, C.S., Niles, P., and Rogalsky, C.J., "Efficient Simulation of Complex Fenestration Systems in Heat Balance Room Models," *12th International Conference of the International Building Performance Simulation Association*, Sydney, Australia, 2011 (Code 93272), pp. 2851, 2858.

[3] Barnaby, C.S., Wright, J.L., and Collins, M.R., "Improving Load Calculations for Fenestration with Shading Devices," *ASHRAE Transactions*, Part 2, Vol. 115, 2009, pp. 31, 44.

[4] Hatton, A.P., and Turton, J.S., "Heat transfer in the thermal entry length with laminar flow between parallel walls at unequal temperatures," *Int. J. Heat Mass Transfer*, Vol. 5(7), 1962, pp. 673-679.

[5] Mitrović, J., Maletić, B., and Bačlić, B.S., "Some peculiarities of the asymmetric Graetz problem," *Int. J. Eng. Science*, Vol. 44(7), 2006, pp. 436-455.
DOI: 10.1016/j.ijengsci.2006.02.003

[6] Mitrović, J., and Maletić, B., "Effect of thermal asymmetry on heat transfer in a laminar annular flow," *Chem. Eng Technology*, Vol. 28(10), 2005, pp. 1144-1150.
DOI: 10.1002/ceat.200600069

[7] Coelho, P.M., and Pinho, F.T., "Fully-developed heat transfer in annuli with viscous dissipation," *Int. J. Heat Mass Transfer*, Vol. 49(19-20), 2006, pp. 3349-3359.
DOI: 10.1016/j.ijheatmasstransfer.2006.03.017

[8] Lundberg, R.E., McCuen, P.A., and Reynolds, W.C., "Heat transfer in annular passages – Hydrodynamically developed laminar flow with arbitrarily prescribed wall temperatures or heat fluxes," *Int. J. Heat Mass Transfer*, Vol. 6(6), 1963, pp. 495-529.

[9] ANSYS, 2011, "ANSYS FLUENT User's Guide," ANSYS, Inc., Canonsburg, PA.

[10] ANSYS, 2011, "ANSYS FLUENT Theory Guide," ANSYS, Inc., Canonsburg, PA.

[11] Celik, I.B., Ghia, U., Roache, P.J., Freita, C.J., Coleman, H., and Raad, P.E., "Procedure for estimation and reporting of uncertainty due to discretization in CFD Applications," *J. Fluids Eng.*, vol. 130, 2008, pp. 0780011-0780014.
DOI: 10.1115/1.2960953

[12] Roberts, A., and Barrow, H., "Turbulent Heat Transfer to Air in the Vicinity of the Entry of an Internally Heated Annulus," *Proc Instn Mech Engr*, Vol 182, Pt 3H, 1967, pp. 268-176.

[13] Malik, M.R., PhD Thesis, "Prediction of Laminar and Turbulent Flow Heat Transfer in Annular Passages," 1978, Iowa State University.